Trans Indian Inst Met (2019) 72(10):2877–2891
https://doi.org/10.1007/s12666-019-01764-3

TECHNICAL PAPER

Processing Techniques to Develop Metallic Materials with Superior Mechanical Properties

Arun Kumar[1] · Uma Thanu Subramonia Pillai[1] · Amirthalingam Srinivasan[1]

Received: 14 October 2018 / Accepted: 13 June 2019 / Published online: 13 July 2019

Abstract Components made of metallic materials with superior mechanical properties are of high demand in this modern era. Different processes and techniques are used to get improved mechanical properties of the metallic materials such as semisolid casting, ultrasonic melt treatment, friction stir processing and severe plastic deformation processes. It is observed that the selection of a particular method for processing of a component mainly depends on the factors, viz., material properties, size and shape of component and other economic factors. The parameters to be optimised for the productive operation of each of these processes are also reported in this paper.

Keywords Severe plastic deformation · Friction stir processing · Ultrasonic melt treatment · Superior mechanical properties

1 Introduction

Metallic-based materials with high specific strength, temperature resistant, hardness and toughness are demanded by various industries such as aeronautics, automobiles, nuclear reactors and space shuttles [1–3]. Conventional methods like casting process especially gravity and die castings are the major fabrication methods for metals and alloys because of its ease and economical factors [4–11]. However, conventional casting techniques produce components which suffer from defects like agglomeration, non-uniform distribution of reinforcements, porosity, etc. Processing techniques such as, ultrasonic melt treatment, semisolid processing and disintegrated melt deposition are examples of innovations in conventional casting processes to overcome these drawbacks to a certain limit [10–17].

Although the techniques mentioned above are able to make components from advanced materials, further processing is very much needed to obtain specific mechanical properties demanded by industries. This is achieved by inducing high strain into the material using various forming processes such as rolling, forging, extrusion and drawing. These forming processes are associated with size and shape of the components. But, near net shape components produced using advanced fabrication techniques do not require considerable change in dimensions. Thus, processes such as friction stir processing (FSP) and severe plastic deformation (SPD) processes have been developed to improve the mechanical properties by grain refinement with minimal or no change in the cross-sectional dimensions [18–21]. Moreover, SPD techniques have proved to impose much higher strain compared to conventional forming methods. Various SPD processes, viz., accumulative roll bonding (ARB), constrained groove pressing (CGP), equal-channel angular processing (ECAP) and high-pressure torsion (HPT) used for processing near net shape components are also discussed in this paper. The selection of these SPD techniques depends on the shape of the components to be processed; bars and rods are processed using ECAP, discs using HPT and sheets using ARB and CGP [22–26].

This paper mainly reviews on the advancement made in fabrication techniques and severe plastic deformation processes adopted for the production of components using metallic materials.

✉ Uma Thanu Subramonia Pillai
utspillai@rediffmail.com

[1] Materials Science and Technology Division, CSIR – National Institute for Interdisciplinary Science and Technology (NIIST), Trivandrum 695019, India

2 Semisolid Processing

Although conventional casting techniques are suitable for fabrication of bulk components, these components fabricated using conventional casting often contain dendritic morphology and internal structural defects that lead to poor mechanical properties. Grain refinement, rapid solidification and semisolid processing are some of the ways by which dendritic formation can be altered. Besides, helping in achieving a nondendritic structure, semisolid processing also helps in reducing porosity, macro-segregations and forming efforts. In semisolid processing, the material is processed in partially solid and partially liquid state; thus, nonferrous alloys such as aluminium, magnesium and copper with sufficient melting temperature range and good fluidity are more suited [27–30]. It is now well established that the shearing action (either through mechanical or electromagnetic means) during the solidification of the alloys results in breaking up of the dendrites and suspension of globules of primary phase in the liquid [31]. The solidification occurring in the semisolid die casting process can be considered in two stages. Firstly, primary globules are nucleated and grow in the slurry maker; secondly, slurry is solidified, which involves non-equilibrium eutectic reactions. In addition, uniform distribution of primary particles and solute elements owing to the shearing action imposed on the slurry leads to homogeneous nucleation and growth of secondary grains [32–34]. The ability of semisolid processes such as thixocasting, where the precast billet is heated to the semisolid range, and rheocasting, where the melt is cooled down to reach the semisolid range, to alter the dendritic morphology has been studied by various researchers. Microstructures of the squeeze and rheocast AZ91 as well as the thixocast AZ80 are presented in Fig. 1, and it can be observed that shape and distribution of the different phases are dependent on the casting route. For squeeze-cast structure, solidification starts with the nucleation of the primary α-Mg globules; however, forced nucleation of α-Mg and globular growth is exhibited in rheocast and thixocast structures. But, for the thixocast structure, eutectic phase is also present inside the globules [32]. Similarly, semisolid die casting of AZ91 alloy exhibits a uniform distribution of primary α-Mg globules as observed in AZ80 [33]. Rheocasting of 5052 Al alloy has resulted in a nondendritic microstructure with homogeneous distribution of primary α particle. Moreover, UTS of 191 MPa and 7.5% elongation is obtained for rheo-gravity cast 5052 alloy compared to UTS of 156 MPa and 4.1% elongation obtained after conventional gravity cast 5052 alloy [34].

Parameters that alter the final microstructure in semisolid casting are the pouring temperature, stirring speed and time. For example, a decrease in the stirring temperature results in an increase in the viscosity and solid fraction of the slurry. It is observed that for a constant stirring time at lower temperature, due to low fluidity, globules become coarser. So, it is important to optimise the processing temperature to get fine globules in a particular alloy. For example, particle size of primary α Al in Al–Si–Mg–Fe alloy processed using semisolid casting reduces from 110 µm at 650 °C rheocast temperature to 60 µm at 620 °C rheocast temperature. The refinement of primary α has resulted in an increase in UTS from 160 MPa at 650 °C to 188 MPa at 620 °C and elongation from 5.9% at 650 °C to 8.4% at 620 °C for 10% volume fraction of solid. Further increase in volume fraction of solid to 20% at 620 °C has contributed to the increase in UTS to 203 MPa and elongation to 10%. The effect of rheocast processing temperature on elongation and UTS of Al–Si–Mg–Fe alloy is shown in Fig. 2 [35]. Studies show that the optimum rheocast temperature corresponds to the one at which the melt possesses 50 volume fraction of solid. However, it is

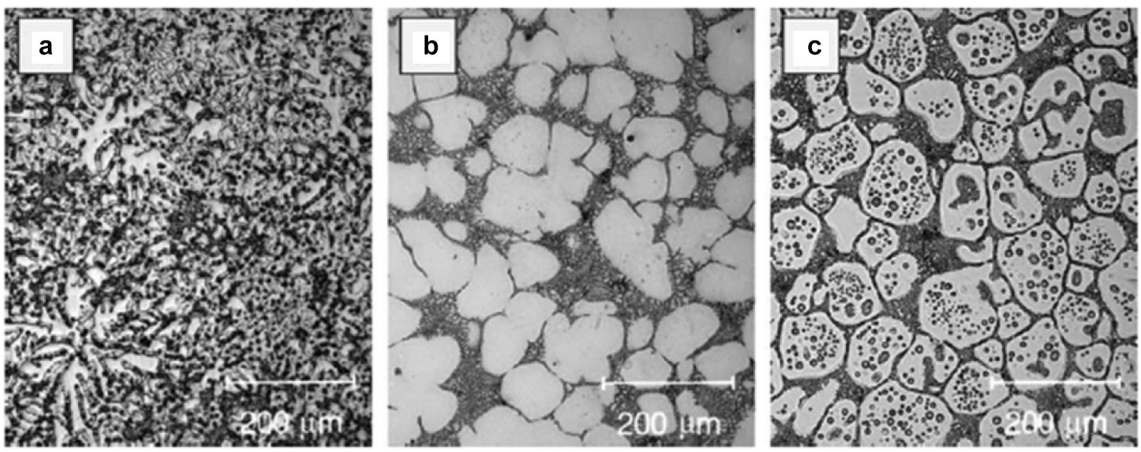

Fig. 1 Microstructures of **a** AZ91 squeeze cast, **b** AZ91 rheocast and **c** AZ80 thixocast [32]

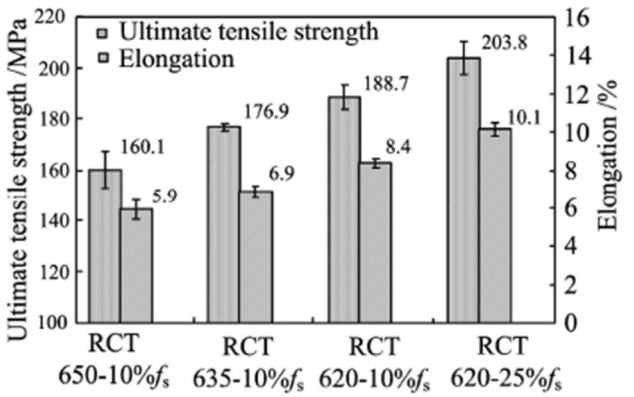

Fig. 2 Effect of rheocast processing temperature on elongation and ultimate tensile strength of Al–Si–Mg–Fe alloy [35]

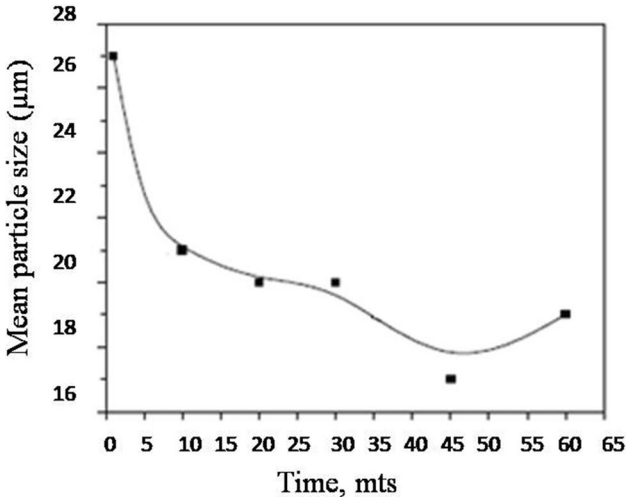

Fig. 3 Plot of mean particle size versus isothermal stirring time (400 rpm) at 615 °C(Al–5.2Si alloy) [41]

to be noted that processing temperature also affects the porosity in the samples. As at higher temperatures, flow will become turbulent and thus increase the amount of entrapped air [36, 37]. But, for the same pouring temperature, stirring of the melt affects the microstructure immensely [38–40]. It has been reported by Liu et al. [38] and Nafisi et al. [39] that for the same pouring temperature in rheocasting of A356 alloy, with and without stirring, finer, uniform and globular primary particles are observed when the melt is stirred [38–40].

Mechanical stirring is used to impose shearing action in the slurry which also melts grain boundaries and breaks up the initial dendritic structure, but the increase in stirring time results in coarsening of primary globules. The mechanical stirring carried out at different stirring speeds and time in Al–5.2Si alloy proves that as stirring speed increases globular primary particle size decreases. In addition, for a constant stirring speed, increase in stirring time leads to decrease in size of primary particles till an optimum time and further increase in time results in coarsening of these particles and this behaviour can be seen in Fig. 3 [41]. Similarly, increase in stirring speed from 100 to 400 rpm in rheocasting of Al–7%Si alloy has resulted in decrease in size of agglomerates. Moreover, it is also reported that with the assistance of stirring, even for a short period of time, a nondendritic structure is obtained [42]. For a constant stirring speed of 300 rpm and different combinations of process parameters, stirring time and temperature of 30 min and 640 °C, respectively, have proved to be most efficient in obtaining uniform distribution of particles in ABOw (aluminium borate whisker) + SiCp-reinforced Al6061 composites. Increase in stirring time from 20 to 30 min leads to a reduction in agglomeration of particles and an increase in UTS from 214 to 293 MPa [43].

The ability of semisolid processing to fabricate components with uniform nondendritic microstructure and excellent mechanical properties is well established by the studies reported above. But, to obtain a nondendritic microstructure, factors such as processing temperature, stirring speed and time must be optimised. This nondendritic microstructure obtained using semisolid casting finally leads to better mechanical properties. However, obtaining a nondendritic microstructure is no easy process as it is very difficult to maintain a semisolid processing temperature as most of the alloys have a narrow range of mushy state.

3 Ultrasonic Melt Treatment

Recently a new approach has been applied to the processing of alloys and composites with ultrasound for producing high-quality products with minimal defects and better mechanical properties. Ultrasonic treatment of the melt prior to casting results in a nondendritic structure as obtained in a semisolid casting and better dispersion of particles and reduction in porosity to a great extent is also possible [44–46]. The alternating pressure above the threshold results in the cavitation of bubbles which act as the nuclei for solidification degassing and deagglomeration. The bubbles thus formed behave differently, as some of them oscillate with the frequency of the applied ultrasonic field, whereas some cavitation bubbles start to grow due to the tensile pressure of a sound wave and the unidirectional hydrogen diffusion into the bubble and some of the bubbles do not have a chance to be filled with the dissolved hydrogen and therefore collapse during the compression stage of a sound wave. Collapsing bubbles create very fine fragments and the process repeats with these fragments by the chain-reaction mechanism. These

processes occur spontaneously, during a few periods of a sound wave [47, 48]. The effect of ultrasonic treatment (UT) of melts prior to casting by various researchers has been discussed below.

UT of AZ91 magnesium alloy has resulted in refinement of α-Mg phase and intermetallic phases $Mg_{17}Al_{12}$, Mg_2Si and MnFeAl(Si). SEM image of AZ91 alloy processed with and without UT in Fig. 4 reveals the refinement of intermetallic phases with UT of AZ91. The refinement of intermetallic phase attributes to the improvement in tensile strength of the sample from 94 MPa without UT to 165 MPa with 60% ultrasonic power [49].

Similarly, UT of ADC12 (A383) die cast alloy has resulted in the transformation of long plate-like Fe intermetallic phases of about 200 μm length to a much refined globular form of size less than 15 μm. Moreover, nucleation undercooling (measure of nucleation efficiency) is reduced from 2.9 to 0.4 °C with UT which implies that UT stimulates the nucleation process [50]. It is also observed that the UT close to the melting temperature refines the solidification microstructure owing to the solidified alloy formed on ultrasonic horn (as it has superior cooling potential). The phases that are broken down to fine parts due to cavitations and acoustic streams serve as sites for crystallisation [50–52]. Although, UT is suitable for both alloys and composites alike, the particles present in composites act as heterogeneous nucleation sites for formation of cavitation bubbles, thus enhancing the effects of UT. The presence of reinforcement particles in the slurry increases the rate of formation of cavitation bubble and agitation of melt in areas near to the sonotrode tip. Even though cavitation and agitation helps in improving solidification, vigourous agitation of the melt may result in undesirable defects in castings, such as oxide bifilm formation, porosity or unfavourable changes to the microstructure [53–56].

The above discussion points out that UT of the melt helps in achieving microstructures similar to the nondendritic microstructure obtained with semisolid castings in all alloys and composites irrespective of their mushy zone range. Although UT is able to induce grain refinement in both alloys and composites, the particles present in composite act as nucleation sites for formation of cavitation bubbles and thus enhances the effects of UT. This in turn results in the uniform distribution of particles in composites which further leads to better mechanical properties.

4 Friction Stir Processing (FSP)

FSP technique is a promising solid-state mechanical processing method for surface microstructural modifications of materials and fabrication of surface composites. FSP is able to induce a wrought microstructure in a component and reduce many of the casting defects such as porosity and inhomogeneous microstructure. The versatility it offers and environment friendliness makes FSP a favourite processing route for structural modifications of the material [57–59]. Mishra et al. [60] have developed FSP as a means for microstructural modification of the surface of materials and now it is also used to develop surface composites. The basic working principle of FSP is same as that of friction stir welding (FSW). FSW is a solid-state joining process in which the heat generated by the friction between rotating tool and workpiece softens the area near the tool. In FSP, a rotating tool is forcefully passed over the material surface along a line where modifications are required (Fig. 5 shows the schematic representation of friction stir processing) [60, 61]. The temperature generated during FSP affects grain size and thus the mechanical properties. The temperature decreases from the surface towards the bottom of the material and as a result, grain size reduces and hardness increases, since at higher temperatures softening of the

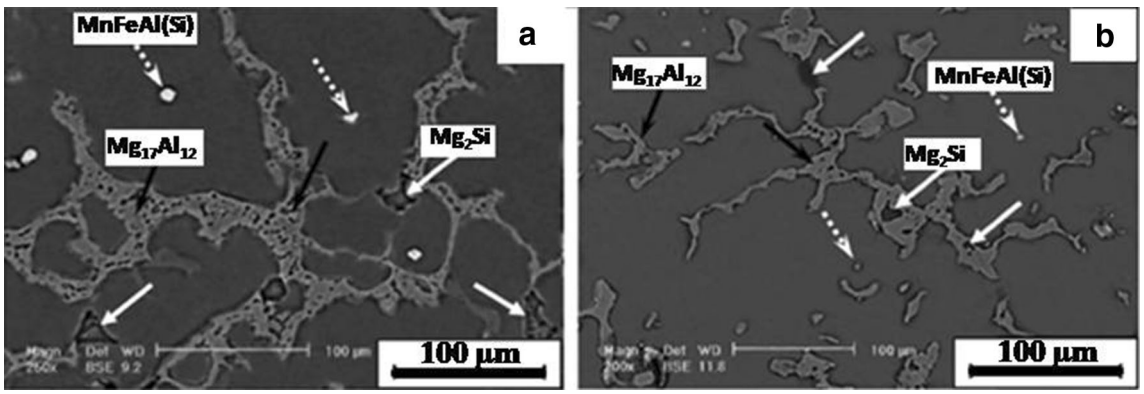

Fig. 4 SEM micrographs of different intermetallic phases observed in AZ91: **a** without ultrasonic treatment and with ultrasonic treatment for 5 min [49]

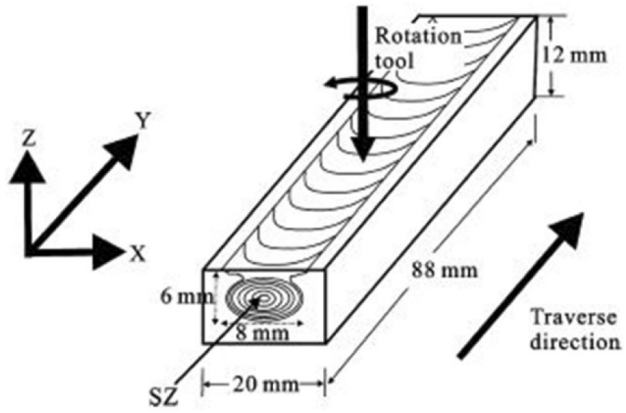

Fig. 5 Schematic representation of friction stir processing [72]

matrix occurs and grain growth takes place [62]. Elimination of casting defects such as porosity and cold flake, grain refinement and uniform dispersion of particles offered by FSP help the materials processed to obtain better mechanical properties. For example, Saito et al. [63] have reported grain refinement of 1050 aluminium alloy using FSP and the reduction in grain size from 8 to 2 μm after FSP has resulted in higher microhardness in the processed region [63]. The hardness of aluminium die cast alloy increases from 90 Hv to 110 Hv due to FSP and tensile strength increases almost 1.7 times after FSP, a 30% increase in ultimate and yield strength and a fourfold increase in ductility is observed for FSPed Al 2285 alloy [64, 65]. Similarly, FSP has been used as a means to successfully split-up the coarse eutectic β-$Mg_{17}Al_{12}$ phase in AZ91 alloy [66] and the dispersion of Si particles into the α-matrix in A356 alloys [67] resulting in an increase in mechanical strength, grain refinement and particularly ductility [66, 67]. After one FSP pass, grain size of AZ31 is reduced from 75 μm to 100–300 nm and microhardness is increased from 50 to 120 Hv [68]. The microstructure of FSPed A356 and A319 show uniform distribution of secondary phases with no visible casting defects. The optical microstructures of A319 before and after FSP shown in Fig. 6 exhibit the dispersion of particles after the FSP. Tensile strengths of as-cast A319 and A356 increase from 154.8 and 139.5 MPa to 300 and 173.6 MPa, respectively, after FSP [69].

Although FSP is suitable in altering the surface microstructure of materials, it is also used for fabrication of surface composites. Mishra et al. [70] have successfully fabricated Al-SiC particulate surface composite using FSP technique. Out of the different target depths and traverse speeds used, a target depth of 2.03 mm with a tool traverse speed of 25.4 mm min^{-1} has resulted in the incorporation of up to 27% of SiC by volume into the base matrix and has resulted in successful bonding between particles and the matrix. Figure 7 shows the perfect bonding between the particle and the matrix [70].

Similar observations are made by Morisada et al. [71] as multiwalled carbon nanotubes (MWCNTs) are incorporated into AZ31 magnesium alloy using FSP with an optimum tool traverse speed of 25 mm min^{-1}. Both the studies suggest that there exists an optimum tool traverse speed to obtain perfect dispersion of the particles. A higher traverse speed is too fast to produce enough heat flow to produce suitable viscosity in the matrix to allow the incorporation of particles [71]. Al–Al_3Ti nanocomposites are fabricated from Al–Ti elemental powders with the aid of high temperature developed, due to the friction between the workpiece and tool during FSP, which in turn leads to in situ formation of the intermetallic Al_3Ti phase. The composite has shown 63% increase in Young's modulus compared to aluminium, due to the grain refinement and uniform distribution of Al_3Ti phase obtained after FSP [72]. The number of FSP passes has a huge impact on uniform distribution of particles in the matrix, grain refinement and mechanical properties. It is reported that increase in number of FSP passes has resulted in better distribution of Al_2O_3 nanoparticles in Al 6082 alloy. Moreover, after four FSP passes, grains having size less than 300 nm and an increase in microhardness is observed [73]. Likewise, Lee et al. [74] have reported uniform distribution of SiO_2 nanoparticles in AZ61 Mg alloy after four FSP passes. Figure 8 shows the SEM micrographs of FSPed AZ61 Mg alloy reinforced with uniformly distributed SiO_2 nanoparticles [74].

The above discussion shows that, although FSP has been introduced as a surface modification process, it is now currently used by researchers for fabrication of surface composites also. It has also been reported by researchers that mechanical properties and microstructure of the processed zone can be effectively controlled by optimising different parameters. Further, increase in number of passes has resulted in a much refined microstructure in alloys and homogeneous distribution of particles in composite materials.

5 Severe Plastic Deformation (SPD)

The demand for ultra-fine-grained (UFG) materials by industries requires processes that are capable of inducing high strain into the materials. Conventional forming operations such as rolling, extrusion and forging are able to impose strain less than around two. However, strain higher than 2 is possible with multi-pass rolling and extrusion, but, the end product being so thin, it is not suitable for industrial applications [75, 76]. Thus, alternate processes, viz., SPD techniques such as equal-channel angular process

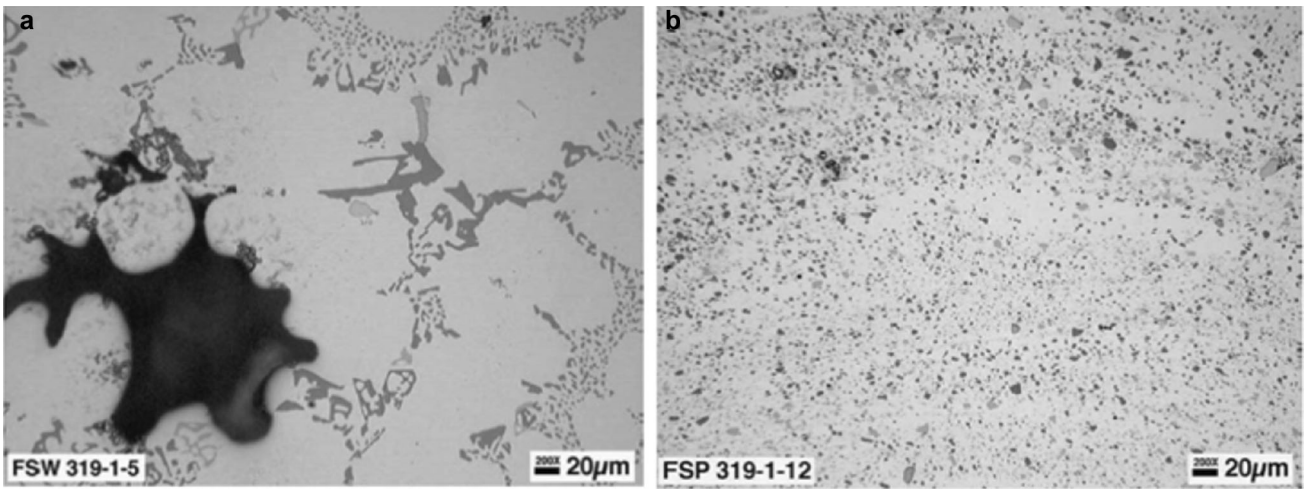

Fig. 6 Optical microstructures of A319 (**a**) as-cast (**b**) FSPed [69]

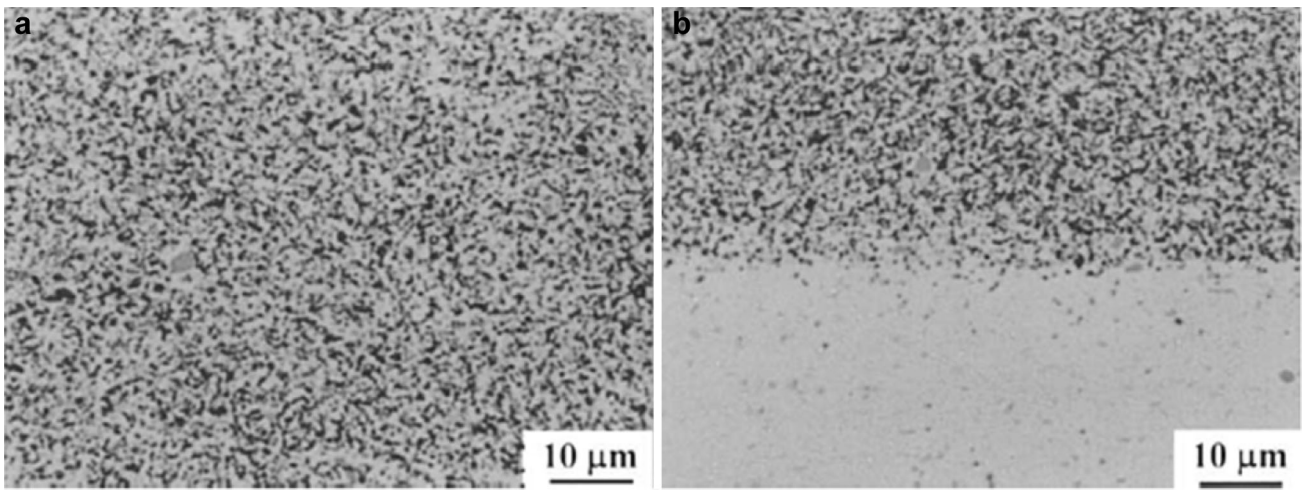

Fig. 7 Optical micrographs **a** homogeneous dispersion of SiC particles (27 vol%) in Al alloy matrix and **b** perfect bonding between substrate and surface composite [70]

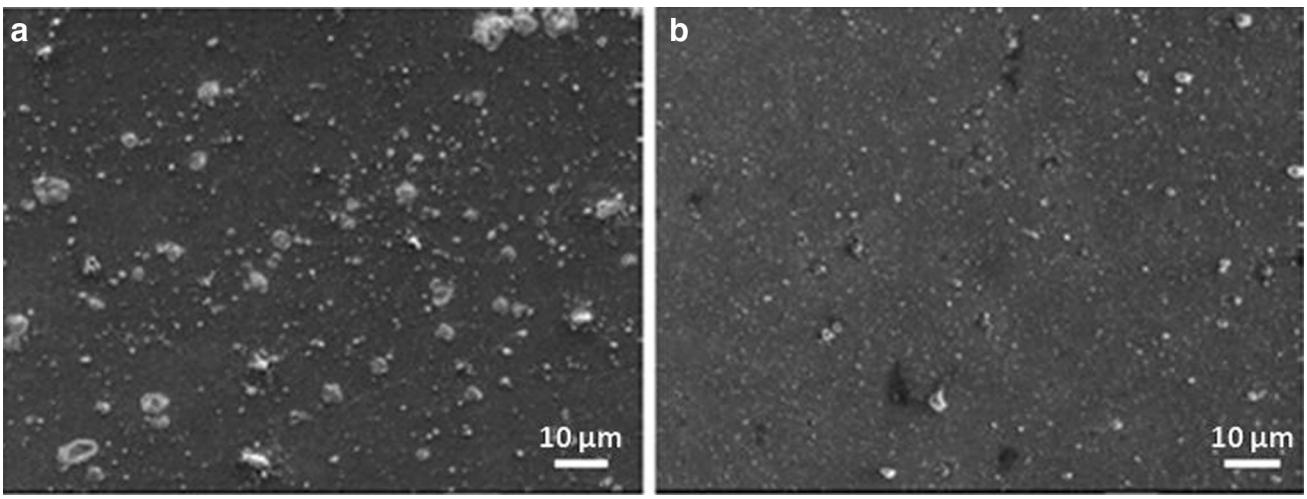

Fig. 8 SEM micrographs of AZ61–5vol% SiO_2 showing the particle dispersion after: **a** one FSP pass, **b** four FSP passes [74]

(ECAP), high-pressure torsion (HPT), accumulative roll bonding (ARB), constrained groove pressing (CGP), etc., have been developed to meet the demands. Unlike in conventional forming operations such as forging, extrusion and rolling, materials that are processed using SPD do not undergo a change in cross-sectional dimension. This provision thus allows the sample to be processed for multiple times to obtain higher strains without any considerable change in the cross-sectional dimension. Besides grain refinement, SPD offers significant reduction in porosity and a uniform microstructure. Some of the common SPD techniques are discussed below:

5.1 Equal-channel angular processing (ECAP)

In equal-channel angular processing (ECAP) technique, the component is pressed through a die using a plunger. The sample while passing through the die experiences simple shear as shown in Fig. 9. Although relatively high amount of strain is introduced in the component, there is no significant cross-sectional change. Moreover, it is an attractive technique due to various factors as it is comparatively easy to fabricate and use an ECAP die and it also helps in imposing high strains. The ECAP samples are more favoured as they can be scaled-up to produce large bulk materials which find application in various industries such as biomedical and aerospace industries [75–77].

ECAP can be performed with different processing routes (A, B_A, B_C and C) which has a significant effect on the microstructure and shear planes on material under consideration. Rotation of billet is not allowed in route A, rotation of billets in alternate or same directions is followed in B_A and B_C, respectively, and 180^0 rotation of the billet is followed in route C. It has been reported that different processing routes induce shearing patterns into the components resulting in macroscopic distortions and development of a homogeneous and equiaxed UFG microstructure. The close examination of the various processing routes has revealed the shearing characteristics associated with these routes and it is reported that the route B_C is more favoured over other routes as homogeneous deformation of the sample along all the directions is possible with this route [78–81]. Similar results are also reported by Stolyarov et al. on the study of the effect of ECAP routes B_C, B_A and C on titanium. Equiaxed grains of 260 nm sizes are achieved with route B_C compared to the elongated grains obtained with routes B_A and C. Although, improved mechanical properties are achieved with routes B_A and C, the route B_C is considered as the best due to the better surface quality and the equiaxed grains it produces [82]. Although Bc is the best route for better grain refinement, it is observed that the change in microhardness values is negligible with respect to different routes, but higher and lower strength values are achieved with respect to routes A and C [83, 84].

Further in ECAP, the angle of the die plays a major role in imposing strain on the work piece. The strain induced on the ECAPed sample is mainly dependent on the angles Φ, between two parts of the channel, and Ψ, between the outer arcs of curvature. Figure 10 shows the dependency of strain imposed on Φ and Ψ. It is clear that the strain increases with a reduction in Φ and Ψ [85, 86].

The effect of ECAP on grain refinement and mechanical properties has been studied by many researchers. ECAP studies on aluminium have exhibited a considerable reduction in grain size to 650 nm leading to significant improvement in UTS from 71 to 180 MPa after four passes [87]. Similarly, the grain size of AM30 Mg alloy is

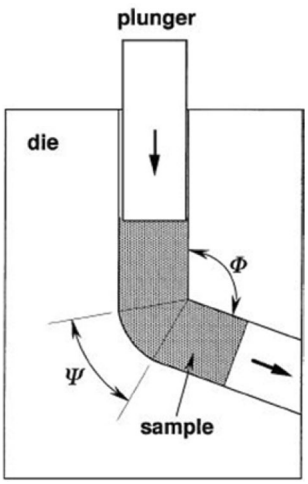

Fig. 9 Schematic diagram of an ECAP die [79]

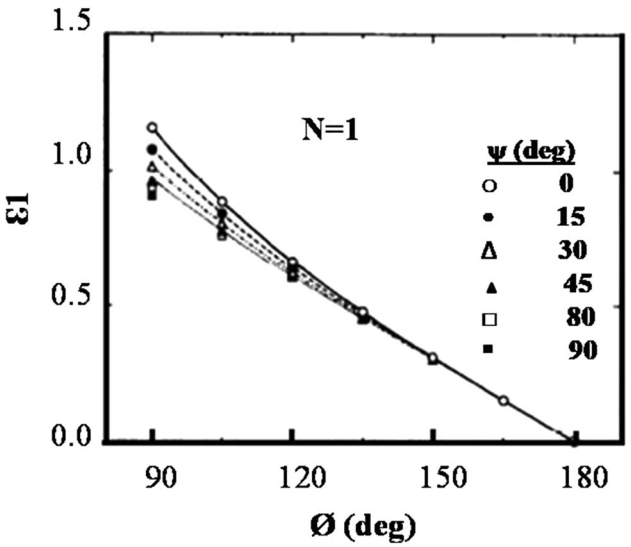

Fig. 10 Variation of strain, $\varepsilon 1$ for a single passage through the die ($N = 1$) showing the dependence on Φ and Ψ [85]

reduced from 20.4 μm to 3.9 μm after four ECAP passes and subsequent passes lead to an improvement in grain size uniformity [88].

Solid solution strengthening, precipitation strengthening and grain boundary strengthening are the major strengthening mechanisms in ECAP-processed materials. However, Chung et al. have reported the absence of peak shifts in X-ray diffraction which implies that ECAP has no effect on the lattice parameters, underlying that solid solution strengthening is not significant. Similarly, the precipitate size is only reduced to 1 μm after six ECAP passes which is not enough to offer an apparent strengthening. Thus, precipitate strengthening is also not the key strengthening mechanism. But, ECAP processing significantly reduces the grain size; thus, grain boundary strengthening is the major factor in increasing the strength in ECAPed materials [89, 90]. However, in certain studies, it is observed that the reduction in grain refinement achieved with ECAP has not resulted in corresponding increase in strength. For example, the grain size of AZ61 is reduced from 24.4 μm to 8.4 μm, but the yield strength is reduced after eight ECAP passes using Bc route. This demonstrates that although ECAP proves to be a successful method in refining the grains, it is not capable of improving the strength in AZ61 alloy. This is because of the fact that texture softening is predominant over strengthening due to grain refinement in AZ61 [91, 92]. This behaviour is also observed in certain other Mg alloys by researchers. Likewise, grain size of AM60 alloy is reduced from 19.2 to 2.3 μm after six ECAP passes, but yield stress and UTS increase till two passes and decrease with further processing [93]. Grain size of AZ31 is reduced with increase in number of passes, but due to texture softening, the strength is decreased [94].

Although high number of passes is not possible in metal matrix composites, ECAP is effective in achieving grain refinement and improved mechanical properties in composites too. Al 6061 alloy and Al 6061–10% Al_2O_3p composite after eight ECAP passes have resulted in refinement of grain size to 300 nm. In addition, the stress strain behaviour of the composite presented in Fig. 11 is a clear indication of the high mechanical strength along with considerable ductility achieved after ECAP [95]. The grain size of Al-5%SiCp is reduced from 45 to 8 μm and microhardness is increased from 29 to 48 Hv after two ECAP passes, similarly, grain size of Al-5%SiCp is reduced from 45 to 16 μm and microhardness is increased from 44 to 50 Hv after first pass [96]. Four ECAP passes in Al-5% graphite composite have resulted in UFGs of 300 nm, a twofold increase in hardness and increase in strength from 97 to 249 MPa [97]. Maa et al. [98] have used ECAP to successfully break SiC whiskers without failing the aluminium matrix in Al-15% SiC composite and

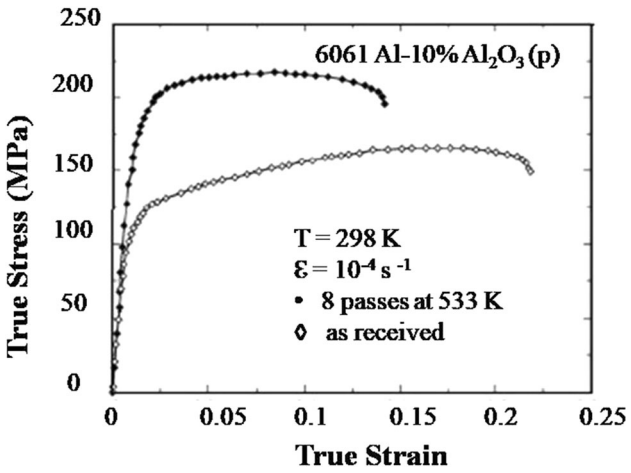

Fig. 11 Stress–strain curve of the 6061Al–10% Al_2O_3(p) composite at room temperature before and after ECAP [95]

it is observed that length of SiC whiskers reduce from 42 to 4 μm after two ECAP passes [98].

After going through the studies reported here, it is clear that ECAP process induces ultra-fine-grained microstructure with the increase in number of passes and of the different processing routes, Bc is the most favourable as homogeneous deformation in all the directions is possible with this route. Moreover, with the help of the studies reported above, it can be seen that the strain imposed on the samples processed by ECAP is mainly dependent on channel angle, angle between outer arcs of curvature, processing route and number of passes. ECAP is promising route compared to other SPD techniques as it is able to handle bulk components or components processed using ECAP can be scaled to bulk components.

5.2 High-Pressure Torsion (HPT)

In ECAP, the strain induced is not dependent on the extrusion pressure, but HPT uses high pressure to obtain torsional straining in the samples being processed (This is shown schematically in Fig. 12.) Samples that are processed using HPT suffer from huge pressure leading to higher amount of deformation and grain refinement compared to ECAP-processed samples. Sample, usually disc-shaped, is placed in the cavity between two anvils, and hydrostatic pressure is applied by the rotation of one of the anvils to achieve torsional straining. HPT is generally used to produce small nano-magnets, arterial stents and various devices for electro-mechanical systems [99–101]. Although higher strains are induced in HPT compared to ECAP, many researchers have reported that the microstructural studies of HPT-processed samples have revealed that the centre of the disc suffers most from torsional straining. The whirlpool-like flow in HPT-processed

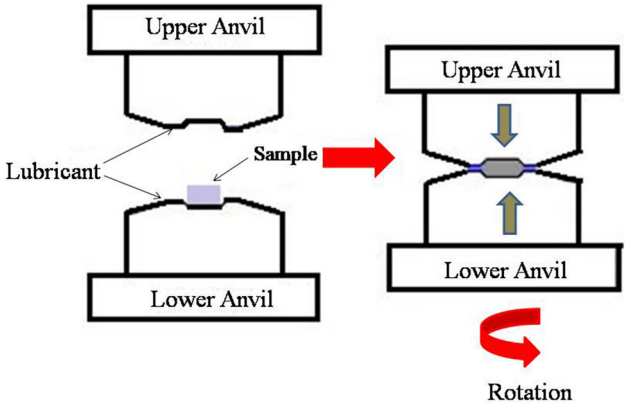

Fig. 12 Schematic illustration of HPT [100]

high-purity aluminium presented in Fig. 13 is in agreement with this statement and is a proof of non-uniform microstructure. It is also clear from Fig. 13 that as the number of turns is increased, the inhomogeneous regions are reduced to a great extent. During HPT, shearing takes place, at a place where friction coefficient is high, resulting in local hardening of the particular point, which in turn reduces the frictional forces and shearing is transferred to the adjacent position [101–103]. The incremental shear strain introduced in HPT-processed material is given by

$$\partial\gamma = (r\,\partial\theta)/h$$

where $\partial\gamma$ is incremental shear strain, r and h are disc radius and thickness and $\partial\theta$ is incremental rotation. Thus, it can be seen from the equation that no strain (theoretically) is introduced at the centre of the disc during HPT. It can also be observed that as distance from the centre increases, strain increases [103].

The microhardness measurements in aluminium and Al–3%Mg–0.2%Sc alloy have shown that initially microhardness is lower at the centre of the sample and increases with distance from the centre to the edge. It is also noted that grain size of Al–Mg–Sc alloy reduces from 0.5 mm to 0.20 μm after ECAP, whereas HPT results in a grain size of 0.15 μm. From Fig. 14, it is clear that after a few turns, microhardness at the centre increases and reaches close to the microhardness at the periphery, and moreover, the inhomogeneity in microstructure is reduced [103, 104]. Although, HPT is widely used as a technique for grain refinement, it is also used for fabrication of metallic and ceramic-based composites. Lee et al. [105] have fabricated Al–7.5% Mg by HPT and it has been reported that microhardness of the composite so developed is almost 50% higher than the composite processed using extrusion [105]. Tokunaga et al. [106] have developed Al-based composite containing fullerene through HPT processing. But, the inhomogeneous distribution of fullerene has resulted in change of mechanical properties with distance from the centre. The composite has shown a microhardness of 39 Hv at the centre and it increases with distance to finally reach saturation at 3 mm away from centre

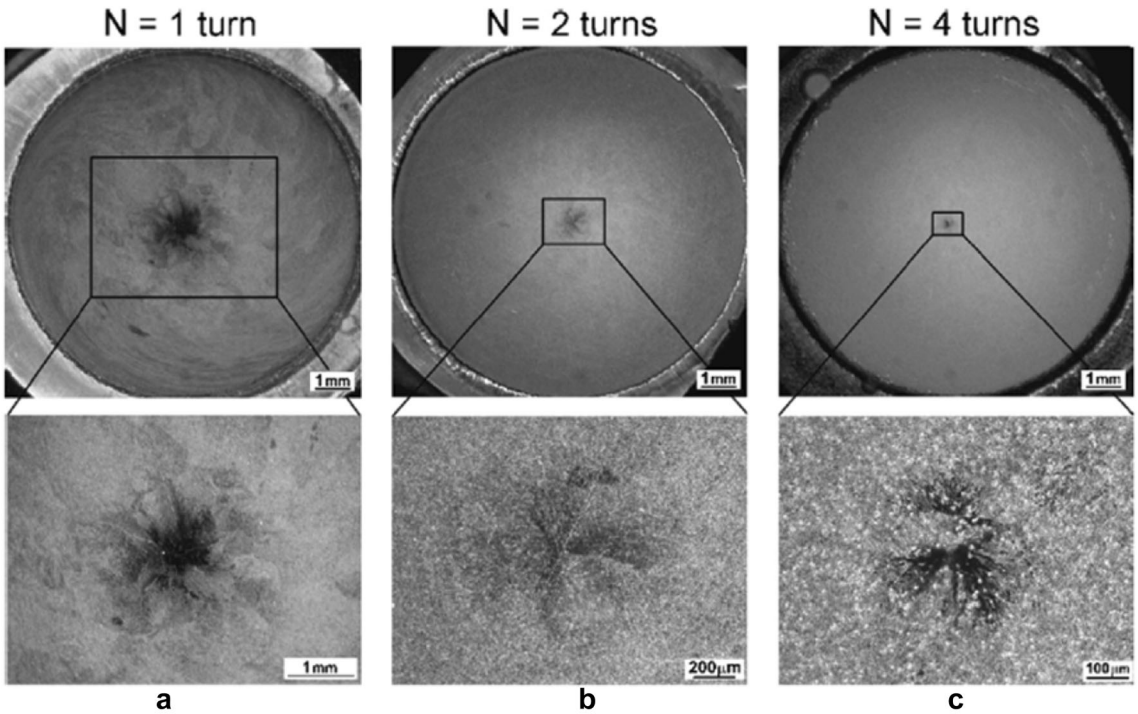

Fig. 13 Upper row : optical micrographs of HPT-processed high-purity aluminium; lower row : the magnified appearance of the central region of each disc [102]

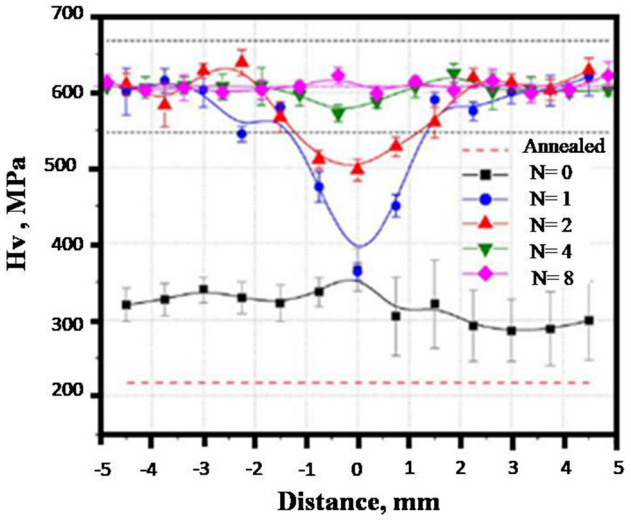

Fig. 14 Microhardness across the diameters of Al samples undergone HPT at a pressure of 1GPa and till eight whole turns [104]

corresponding to 118 Hv [106]. Likewise, Joo et al. [107] have used HPT to process Al-CNT composite and it has been observed that microhardness at the centre is 70 Hv and at 1 mm away from the centre is 85 Hv. Although, it is reported that microhardness of the composite increases with distance from centre, it reaches saturation at 1 mm away from the centre and there is no appreciable increase in hardness beyond 1 mm. Higher tensile strength of 510 MPa is observed for the composite owing to the homogeneous distribution of CNT in the aluminium alloy compared to 255 MPa of aluminium alloy [107]. Although Cu-CNT nanocomposite fabricated using HPT has shown uniform distribution of CNT, microhardness of the composite doesn't change significantly with distance from the centre. Moreover, the initial grain size of 0.5–1.5 μm reduces to 22 nm after HPT processing. The uniform microstructure obtained in Cu-CNT composite is in disparity with the Al-CNT nanocomposites processed by Joo et al. [107]. This is due to the different processing routes adopted; Al-CNT composites are directly fabricated from mixed Al and CNT using HPT, whereas Cu and CNT used in Cu-CNT composite have been ball-milled, consolidated using compaction and finally refined using HPT [108] .

It can be clearly seen from the above discussion that although HPT process is able to induce higher strain into the sample compared to ECAPed samples, inhomogeneous microstructure at lower number of cycles is a major issue. Moreover, unlike ECAP, bulk samples cannot be processed by HPT. In addition, researchers have shown that HPT can also be used for consolidation of powders and fabrication of metal and ceramic-based composites.

5.3 Accumulative Roll Bonding (ARB)

For the continuous production of sheets, plates and strips, conventional rolling process has been a suitable deformation process for centuries. But, rolled products after undergoing multiple passes tend to have cracks at the edges and more over, strain per pass is relatively low. Accumulative roll bonding is an alternative process which is able to overcome these drawbacks to a great extent. In ARB, the surfaces to be joined are cleaned by degreasing and wire brushing and then stacked together, heated and rolled. When the process is continued for a number of cycles, strips get bonded to form a bulk material. Figure 15 gives a clear idea about the ARB processing [109]. Moreover, ARB-processed materials possess ultra-high grain refinement and very high strength (Fig. 16). Thirty-two strips of ultra-low-carbon steel developed using ARB at 50 °C show that the yield and tensile strengths have increased by around 200–300% and it has been further reported that increase in number of layers from 4 to 32 has increased the bonding strength from 52 to 100 MPa. However, cracking of edges, due to state of stress at that location, is observed which limits further processing [110]. Increase in number of cycles during ARB processing increases the dislocation density. At the initial stage, strain hardening is the predominant factor in increase in strength, but as the process continues, grain structure predominates in increase in

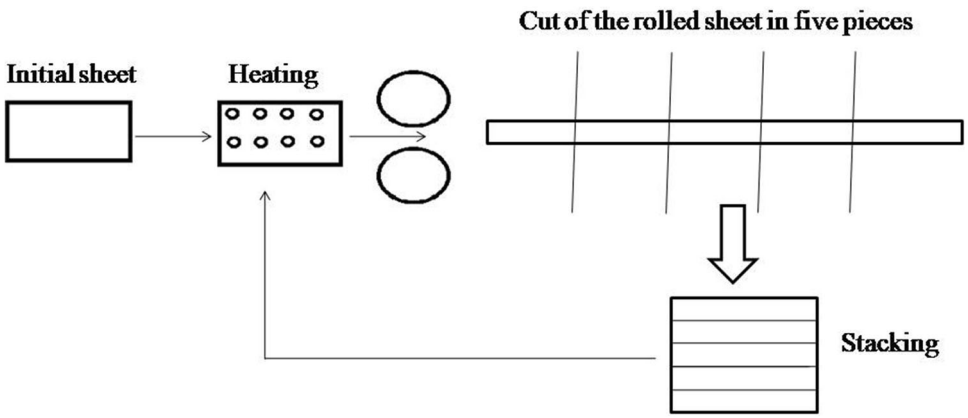

Fig. 15 Schematic representation of ARB processing [113]

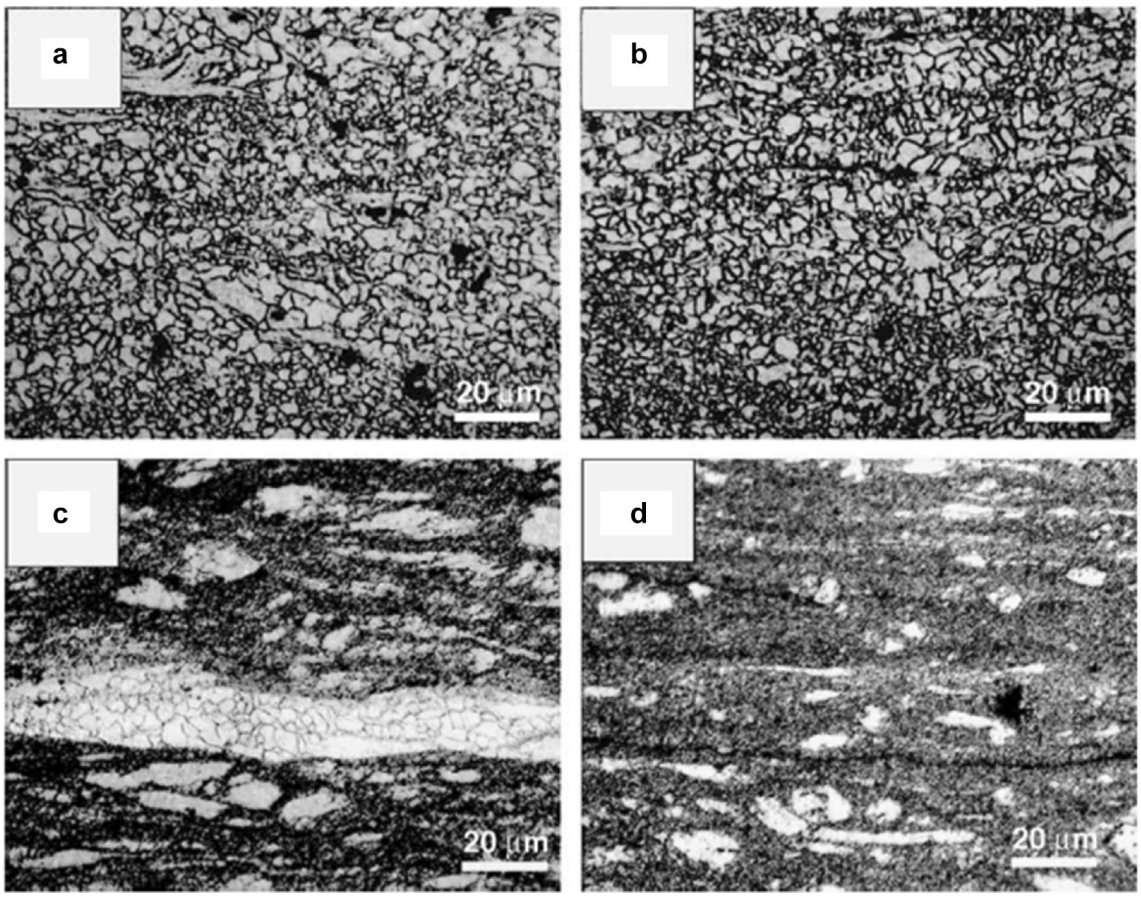

Fig. 16 Microstructures of the alloys processed by accumulative roll bonding. **a** AZ31 single pass; **b** AZ31 four passes; **c** AZ91 single pass; and **d** AZ91 four passes [113]

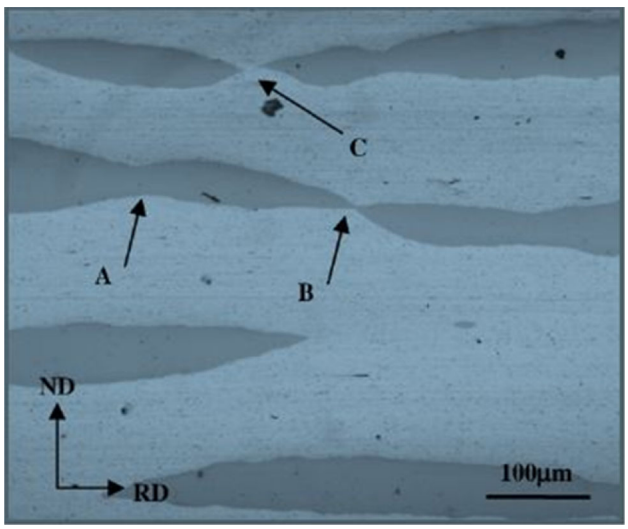

Fig. 17 Optical microstructure shows necking (A) fracturing (B) and departing (C) of Ni layers in longitudinal section of Al/Ni composite after 1 ARB pass [115]

strength. Although ARB processing in some alloys such as AZ31 and AZ91 Mg does not result in significant reduction in grain size beyond the second pass, a homogeneous microstructure is obtained with increase in number of passes as shown in Fig. 17 [111–113]. Usually ARB process is carried out at elevated temperatures with no lubrication, but the use of lubrication in ARB processing of ultra-low-carbon IF steels has revealed that an uniform microstructure is obtained after the first pass itself. Even though, ARB processing without lubrication results in inhomogeneous microstructures in the earlier cycles, increase in number of cycles ensures homogeneity [114].

ARB processing is mainly used for grain refinement of sheets, but it can also be used to fabricate multilayered composites. The different materials are stacked alternatively and rolled for a number of cycle; harder of the two matrices will eventually neck and break due to the deformation process. This phenomenon of necking, breaking and fragmentation is observed in the microstructure of multilayered Al/Ni composites developed using ARB. With the increase in number of cycles, the thickness of both the layers is decreased and finally hard Ni layers are necked and fragmented. The microstructure of Al/Ni composite after first cycle (Fig. 17) exhibits necking, fracturing and

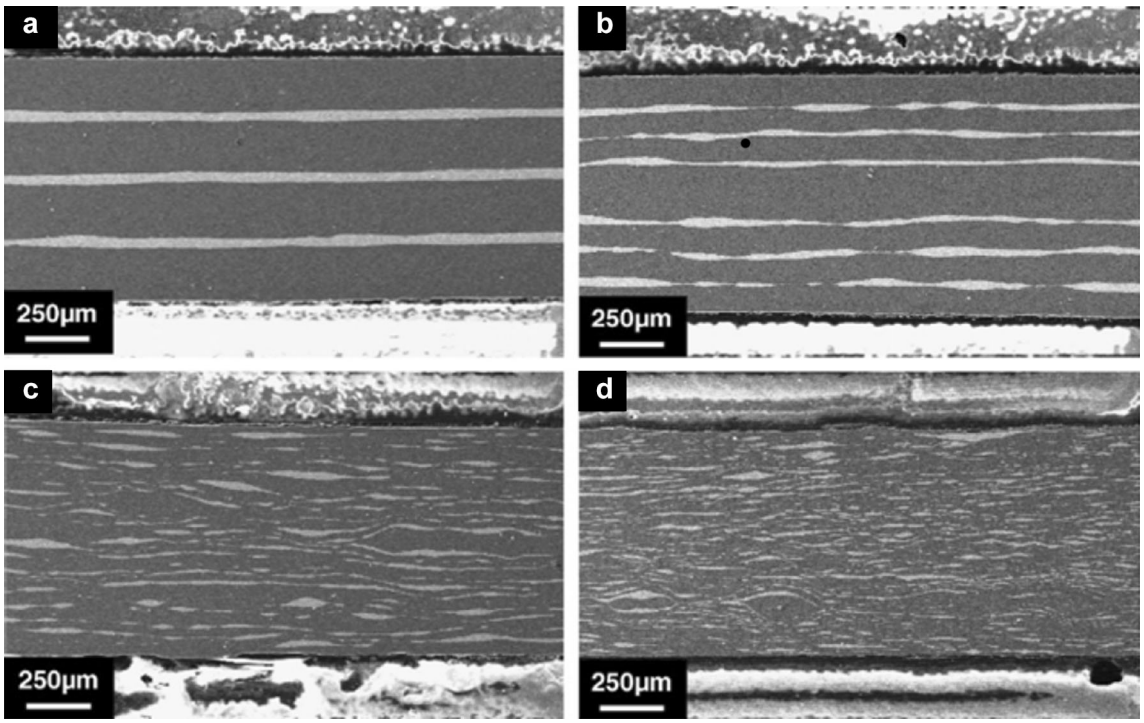

Fig. 18 SEM image of Al/Cu composite cross sections processed using ARB **a** primary sandwich, **b** 1st cycle, **c** 2nd cycle and **d** 5th cycle [116]

departuring of Ni layers [115]. Similar observations are made by Eizadjou et al. [116] on the structure and mechanical properties of multilayered Al/Cu composite produced by ARB process and reported that the composites exhibit an increase in strength and hardness with the increase in number of ARB cycles, but the elongation of the composites decreases compared to the individual metals used. Figure 18 shows the homogeneous distribution of hard Cu layers after five cycles [116].

Thus, it can be deduced that ARB processing proves to be efficient in processing of sheets and is also able to produce multilayered metal composites. Moreover, studies show that the refinement of grains in metallic sheets and homogeneous distribution of the metals in the composites are affected by the number of passes and orientation change between the passes. However, the process should be carried out at a certain temperature for avoiding edge cracking that may happen with the increase in number of passes.

5.4 Constrained Groove Pressing (CGP)

The main drawback of ARB process is that, it needs repeated bonding between the plates and if it fails to obtain perfect bonding between the plates, the bonding interface is likely to deteriorate the mechanical properties of the samples prepared after ARB. Whereas in CGP, sheets are pressed by grooved and flat die repetitively, this induces strain on the sheets. Unlike in ARB, the sheets are not cut

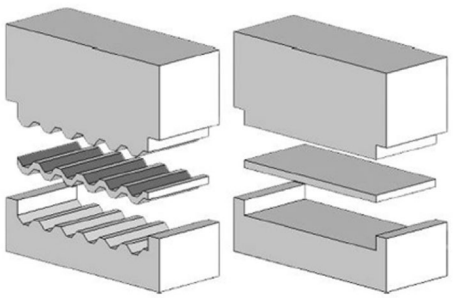

Fig. 19 Schematic of dies used through CGP process, left: grooving die, right: flattening die. [119]

into pieces for the next cycle in CGP, thus bonding is not an issue in CGP. Figure 19 shows dies used for CGP process: grooving die and flattening die. [117, 118]. For obtaining perfect bonding, ARB process is favourable at higher temperatures, whereas CGP can be performed at ambient temperature and there is no cross-sectional change in the case of CGP-processed samples. Although CGP fails to compete with the grain size reduction associated with ARB process, it is efficient enough to obtain materials having UFG microstructure. For example, CGPed low-carbon steel has shown grains with 230 nm size with a strain of 4.64 and ultimate tensile strength of 400 MPa after two passes. CGPed AA3003 alloy has resulted in ultra-fine grains of 580 nm and an increase in tensile strength of 170% compared to annealed sample [119, 120]. TEM images (Fig. 20) of high-purity Al sheets after five

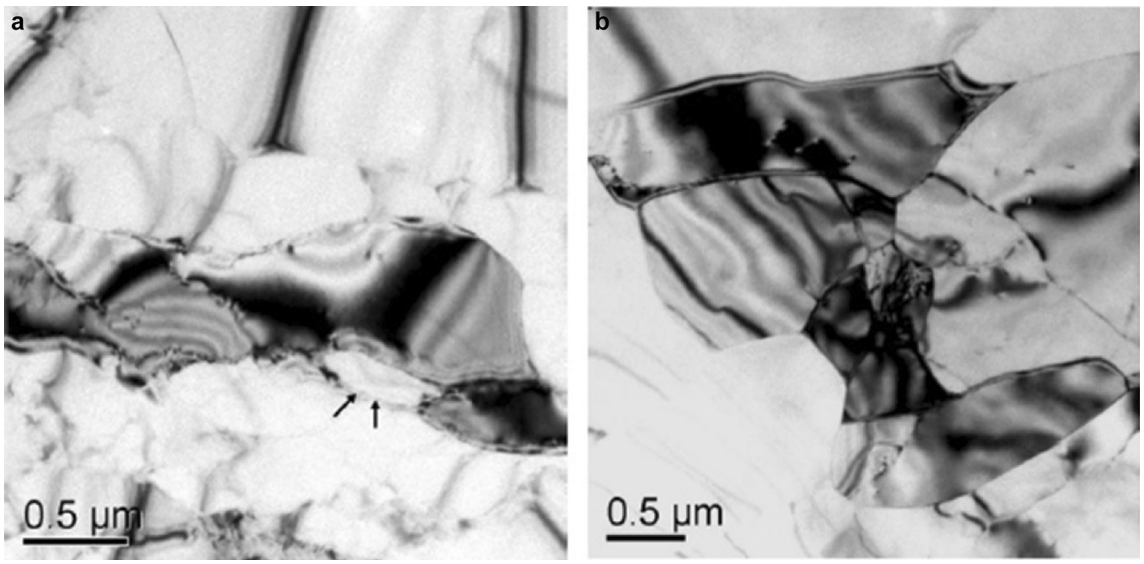

Fig. 20 TEM micrographs of CGP-processed aluminium sheet after **a** first pass and **b** fifth pass [121]

CGP passes reveal that uniform, fine and equiaxed microstructure with well-defined cell boundaries are obtained after fifth pass. However, initially tensile strength is increased from 40 MPa before CGP to 110 MPa after two passes, but, it decreases after third, fourth and fifth passes due to increased number of dislocations [121] .

Similar behaviour is shown by pure nickel sheets processed using CGP as tensile strength, which reduces beyond second pass. This is due to the occurrence of microcracks and elimination of dislocations at higher strains. But, as the number of pass increases, grain size decreases, plastic strain increases and increase in dislocation density is observed. These factors contributes in the initial strengthening mechanism of the CGPed samples; after the first pass, an increase of 60% in tensile strength is observed [122]. Morattaba et al. [123] also reported that CGPed pure Al sheets show remarkable increase in mechanical properties with increase in number of passes. However, appreciable increase in hardness after third and fourth pass is not obtained as the TEM images show dislocation-free cells after the fourth pass. Figure 21 shows the SEM images of the fracture surface, and it is clearly seen that the dimples are more homogeneous and equiaxed after the fourth pass [123].

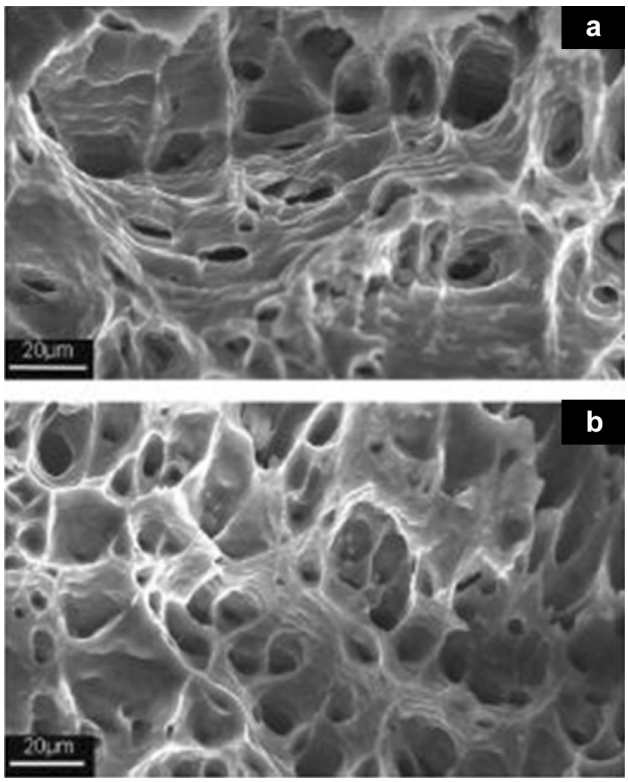

Fig. 21 SEM images of the fracture surface after the first (**a**) and fourth (**b**) pass [123]

6 Conclusion

Conventional casting techniques have been replaced by other advanced processes for production of metallic-based components and composites. It has been concluded that the selection of a particular method for processing of a component depends on factors such as material properties of the component, size and shape of component and economic factors.

1. Semisolid processing is able to produce components made of materials with better mechanical properties owing to the formation of globule-shaped primary particles and the nondendritic microstructure obtained

after semisolid processing. Nonferrous alloys such as aluminium, magnesium and copper with sufficient melting temperature range and good fluidity are used for semisolid processing.

2. Ultrasonic melt treatment is able to produce components with a nondendritic structure much effectively compared to semisolid processing. Further, ultrasonic treatment of melts has added advantage as it also helps in degassing of the melt and deagglomeration of the particles to a great extent. Since ultrasonic treatment is carried out at liquid state, all metallic materials can be processed effectively using ultrasonic treatment.
3. FSP is highly useful in modifying the surface microstructure of cast components and the grain refinement results in better mechanical properties.
4. ECAP is mainly used for inducing high strain into bars or rods and even plate-shaped samples. The components processed can be scaled-up to bulk materials which can be used in wide range of applications.
5. HPT induces much higher strain into the materials than ECAP but limited by the inhomogeniety in microstructure and size of samples it can process. It is favourable for processing of disc-shaped samples and can also be used for production of composites.
6. ARB and CGP techniques are used to impose strain into sheets, plates and strips. ARB can also be used to produce metallic composites. But, ARB requires perfect bonding between the plates and more number of passes to induce higher strain compared to CGP.

References

1. Williamson J R, *Acta Austronautica* **24** (1991) 197.
2. Pater R H, and Curto P A, *Acta Austronica* **61** (2007) 1121.
3. Lau K T, and Hui D, *Composites: Part B* **33** (2002) 263.
4. Koronis G, Silva A, and Fontul M, *Composites: Part B* **44** (2013) 120.
5. Kingery W D, Niki E, and Narasimhan M D, *J. Appl. Phys.* **30** (1959) 301
6. Froes F H, Eylon D, Eichelman G E, and Burte H M, *J. Metals* **32** (1980) 47.
7. Cooper A R, and Eaton J R, *J. American Cer. Soc*. **45** (1962) 97.
8. Coble R L, and Kingery W D, *J. American Cer. Soc.* **39** (1956) 377.
9. Wang H, Fang Z, and Sun P, *Int. J. Powder Metall.* **46** (2010) 45.
10. Rosso M, *J. Mater. Pro. Tech.* **175** (2006) 364.
11. Lee W Y, Stinton D P, *J. American Cer. Soc*. **79** (1996) 3003.
12. Aysha S C P M, Varghese B, and Baby A, *Int. J. Eng. Sci.* **3** (2014) 90.
13. Eskin G I, *Ultrasonics Sonochemistry* **8** (2001) 319.
14. Atamanenko T V, Eskin D G, Zhang L, and Katgerman L, *Metall. Mater. Trans.* A **41A** (2010) 2056.
15. Martinez R A, and Flemings M C, *Metall. Mater. Trans.* A **36A** (2005) 2205.
16. Fan Z, *Int. Mater. Reviews* **47** (2002) 49.
17. Tham L M, Gupta M, and Cheng L, *Mater. Sci. Tech* **15** (1999) 1139.
18. Zehetbauer M J, Stuwe H P, Vorhauer A, Schafler E, and Kohout J, *Adv. Eng. Mater.* **5** (2003) 330.
19. Valiev R Z, *Advan. Eng. Mater.***5** (2003) 296.
20. Azushima A, Kopp R, Korhonen A, Yang D Y, Micari F, Lahoti G D, Groche P, Yanagimoto J, Tsuji N, Rosochowski A, and Yanagida A, *CIRP Annals – Manuf. Tech.* **57** (2008) 716.
21. Zhu Y T, Lowe T C, and Langdon T G, *Scr. Mater.* **51** (2004) 825 .
22. Furukawa M, Horita Z, Nemoto M, and Langdon T G, *J. Mater. Sci.* **36** (2001) 2835.
23. Pippan R, Scheriau S, Hohenwarter A, and Hafok M, *Mater. Sci. Forum* **584–586** (2008) 16.
24. Li L, Nagai K, and Yin F, *Sci. Technol. Adv. Mater.* **9** (2008) 1.
25. Tsuji N, Saito Y, Lee S H, and Minamino Y, *Adv. Eng. Mater.* **5** (2003) 338.
26. Fong K S, Tan M J, Chua B W, and Atsushi D, *Procedia CIRP* **26** (2015) 449.
27. Lou W R, and Suery M, *Mater. Sci. Eng.* **A203** (1995) 1.
28. Spencer D B, Mehrabian R, and Flemings M C, *Metall. Trans.* **3** (1972) 1925.
29. Apaydin N, Prabhakar K V, and Doherthy R D, *Mater. Sci. Eng.* **46** (1980) 145.
30. Molenaar J M M, Katgerman L, Kool W H, and Smeulders R J, *J. Mater. Sci.* **21** (1986) 389.
31. Flemings M C, *Metall. Trans. B* **22** (1991) 269.
32. Kleiner S, Beffort O, Wahlen A, Uggowitzer P J, *J. Light Met.* **2** (2002) 277.
33. Du X, and Zhang E, *Mater. Letters* **61** (2007) 2333 .
34. Lin L S, Sen S S, Meng Z Z, Ping A N, and You-wu M, *Trans. Nonferrous Met. Soc. China* **20** (2010) s758.
35. Burapa R, Janudom S, Chucheep T, Canyook R, and Wannasin J, *Trans. Nonferrous Met. Soc. China* **20** (2010) S857.
36. Haghayeghi R, Zoqui E J, Halvaee A, and Emamy M, *J. Mater. Process. Tech.* **169** (2005) 382.
37. Chao L B, Koo P Y, and Sheng D H, *Mater. Sci. Eng.* **528** (2011) 986.
38. Zheng L, Wei-min M, and Zheng-duo Z, *Trans. Nonferrous Met. SOC. China* **16** (2006)71.
39. Nafisi S, and Ghomashchi R, *Mater. Sci. Eng. A* **174** (2006) 388.
40. Li D N, Luo J R, Wu S S, Xiao Z H, Mao Y W, Song X J, and Wu G Z, *J. Mater. Process. Tech.* **129** (2002) 431.
41. Sukumaran K, Pai B C, and Chakraborty M, *Mater. Sci. Eng. A* **369** (2004) 275.
42. Reisi M, and Niroumand B, *J. Alloy. Cmpd.* **470** (2009) 413.
43. Li-Na G, Lin G, Hong-Wei Z, and Lu-Jun H, *Trans. Nonferrous Met. Soc. China* **21** (2011) S274.
44. Eskin G I, *Adv. Perform. Mater.* **4** (1997) 223.
45. Eskin G I, *Ultrason. Sonochem.* **2** (1995) s137
46. Eskin G I, *Ultrason. Sonochem.* **1** (1994) s59
47. Ramirez A, Qian M, Davis B, Wilks T, and StJohnd D H, *Scripta Materialia* **59** (2008) 19.
48. Eskin D G, *Mater. Sci. Forum* **828–829** (2015) 112
49. Aghayani M K, and Niroumand B, *J. Alloys. Cmpd.* **509** (2011) 114.
50. Khalifaa W, Tsunekawab Y, and Okumiyab M, *J. Mater. Process. Tech.* **210** (2010) 2178.
51. Jian X, Meek T T, and Han Q, *Scripta Mater.* **54** (2006) 893.
52. Li X, Li T, Li X, and Jin J, *Ultrason. Sonochem.* **13** (2006) 121
53. Mirihanage W, Xu W, Ariztondo J T, Eskin D, Fernandez M G, Srirangam P, and P Lee, *Mater. Letters* **164** (2016) 484.
54. Miranda A, Alba-Baena N, McKay B J, Eskin D G, and Shin J S, *Mater. Sci. Forum* **765** (2001) 245.

55. Wang Q, Wang G, Dargusch M S, Qian M, Eskin D G, and StJohn D H , *IOP Conf. Series: Mater. Sci. Eng.* **117** (2016) 12050.
56. Vorozhtsov S A, Khrustalyov A P, Eskin D G, Kulkov S N, and Alba-Baena N, *Russian Physics Journal* **57** (2015) 1485
57. Su J Q, Nelson T W, and Sterling C J, *Scripta Mater.* **52** (2005) 135.
58. Charit I, and Mishra R S, *Mater. Eng. A* **359** (2003) 290.
59. Chang C I, Dua X H, and Huanga J C, *Scripta Mater.* **57** (2007) 209.
60. Mishra R S, Ma Z Y, *Mater. Sci. Eng.* **50** (2005) 1.
61. Mishra R S, Mahoney M W, McFadden S X, Mara N A, and Mukherjee A K, *Scripta Mater.* **42** (2000) 163.
62. Darras B M, Khraisheh M K, Abu-Farha F K, and Omar M A, *J. Mater. Process. Tech.* **191** (2007) 77.
63. Saito N, Shigematsu I, Komaya T, Tamaki T, Yamauchi G, and Nakamura M, *J. Mater. Sci. Letters* **20** (2001) 1913.
64. Nakata K, Kim Y G, Fujii H, Tsumura T, and Komazaki T, *Mater. Sci. Eng. A* **437** (2006) 274,
65. Karthikeyan L, Senthilkumar V S, Balasubramanian V, and Natarajan S, *Mater. Des.* **30** (2009) 2237.
66. Feng A H, and Ma Z Y, *Scripta Mater.* **56** (2007) 397.
67. Sharma S R, Ma Z Y, and Mishra R S, *Scripta Mater.* **51** (2004) 237.
68. Chang C I, Dua X H, and Huang J C, *Scripta Mater.* **57** (2007) 209.
69. Santella M L, Engstrom T, Storjohann D, and Pan T Y, *Scripta Mater.* **53** (2005) 201.
70. Mishra R S, Ma Z Y, and Charit I, *Mater. Sci. Eng. A* **341** (2003) 307.
71. Morisada Y, Fujii H, Nagaoka T, and Fukusumi M, *Mater. Sci. Eng. A* **419** (2006) 344.
72. Hsu C J, Chang C Y, Kao P W, Ho N J, and Chang C P, *Acta Mater.* **54** (2006) 5241.
73. Shafiei-Zarghani A, Kashani-Bozorg S F, Zarei-Hanzaki A, *Mater. Sci. Eng.* **500** (2009) 84.
74. Lee C J, Huang J C, Hsieh P J, *Scripta Mater.* **54** (2006) 1415.
75. Valiev R, *Nature Mater.* **3** (2004) 511
76. Valiev R Z, Estrin Y, Horita Z, Langdon T G, Zehetbauer M J, and Zhu Y T, *J. Mater.* **58** (2006) 33.
77. Langdon T G, *Mater. Sci. Eng. A* **462** (2007) 3.
78. Furukawa M, Iwahashi Y, Horita Z, Nemoto M, and Langdon T G, *Mater. Sci. Eng. A* **257** (1998) 328.
79. Furukawa M, Horita Z, Nemoto M, Langdon T G, *J. Mater. Sci.* **36** (2001) 2835.
80. Furukawa M, Horita Z, and Langdon T G, *Mater. Sci. Eng. A* **332** (2002) 97.
81. Zhu Y T, and Lowe T C, *Mater. Sci. Eng. A* **291** (2000) 46.
82. Stolyarov V V, Zhu Y T, Alexandrov I V, Lowe, Ruslan T C, and Valiev Z, *Mater. Sci. Eng. A* **343** (2003) 43.
83. Tong L B, Zheng M Y, Hu X S, Wu K, Xu S W, Kamado S, Kojima Y, *Mater. Sci. Eng. A* **527** (2010) 4250.
84. Estrin Y, Yi S B, Brokmeier H G, Zúberová Z, Yoond S C, Kimd H S, and Hellmig R J, *Int. J. Mat. Res.,* **99** (2008) 50.
85. Iwahashi Y, Horita Z, Nemoto M, and Langdon T G, *Acta Mater.* **45** (1997) 4733.
86. Nakashima K, Horit Z, Nemoto M, and Langdon T G, *Acta Mater.* **46** (1998) 1589.
87. Raab G J, Valiev R Z, Low T C, and Zhu Y T, *Mater. Sci. Eng. A* **382** (2004) 30.
88. Ramin Jahadi A, Mohammadsedighi A, Hamidjahed, *Mater. Sci. Eng. A* **593** (2014) 178.
89. Chung C W, Ding R G, Chiu Y L, and Gao W, *J. Physics: Conference Phys.* **241** (2010) 1.
90. Xia K, Wang J T, Wu X, Chen G, and Gurvan M, *Mater. Sci. Eng. A* **410–411** (2005) 324.
91. Kim W J, An C W, Kim Y S, and Hong S I, *Scripta Mater.* **47** (2002) 39.
92. Kim W J, Hong S I, Kim Y S, Min S H, Jeong H T, and Lee J D, *Acta Mater* **51** (2003) 3293.
93. Akbaripanah F, Fereshteh-Saniee F, Mahmudi R, and Kim H K, *Mater. Des.* **43** (2013) 31.
94. Kim W J, and Jeong H T, *Mater. Trans.* **46** (2005) 251.
95. Han B Q, and Langdon T G, *Mater. Sci. Eng. A* **410–411** (2005) 430.
96. Ramu G, and Bauri R, *Mater. Des.* **30** (2009) 3554.
97. Saravanan M, Pillai R M, Ravi K R, Pai B C, and Brahmakumar M, *Compos. Sci. Tech.* **67** (2007) 1275.
98. Maa D, Wang J, and Xu K, *Mater. Letters* **56** (2002) 999.
99. Zhilyaev A P, and Langdon T G, *Progr. Mater. Sci.* **53** (2008) 893.
100. Horita Z, and Langdon T G, *Mater. Sci. Eng. A* **410–411** (2005) 422.
101. Zhilyaev A P, Nurislamova G V, Kim B K, Baro M D, Szpunard JA, and Langdon T G, *Acta Mater.* **51** (2003) 753.
102. Kawasaki M, and Langdon T G, *Mater. Sci. Eng. A* **498** (2008) 341.
103. Sakai G, Horita Z, and Langdon T G, *Mater. Sci. Eng. A* **393** (2005) 344.
104. Zhilyaev A P, Oh-ishi K, Langdon T G, and McNelley T R, *Mater. Sci. Eng. A* **410-411** (2005) 277.
105. Lee Z, Zhou F, Valiev R Z, Lavernia E J, and Nutt S R, *Scripta Mater* **51** (2004) 209.
106. Tokunaga T, Kaneko K, Sato K, and Horita Z, *Scripta Mater.* **58** (2008) 735.
107. Joo S H, Yoon S C, Lee C S, Nam D H, S H Hong, and H S Kim, *J. Mater. Sci.* **45** (2010) 4652.
108. Li H, Misra A, Zhu Y, Horita Z, Koch C C, and Holesinger T G, *Mater. Sci. Eng. A* **523** (2009) 60.
109. Saito Y, Utsunomiy H, Tsuji N, and Sakai T, *Acta mater.* **47** (1999) 579.
110. Krallics G, and Lenard J G, *J. Mater. Process. Tech.* **152** (2004) 154.
111. Shaarbaf M, and Toroghinejad M R, *Mater. Sci. Eng. A* **473** (2008) 28.
112. Huang X, Tsuji N, Hansen N, and Minamino Y, *Mater. Sci. Eng. A* **340** (2003) 265.
113. Pe´rez-Prado M T, del Valle J A, and Ruano O A, *Scripta Mater.* **51** (2004) 1093.
114. Kamikawa N, Sakai T, and Tsuji N, *Acta Mater.* **55** (2007) 5873.
115. Min G, Lee J M, Kang S B, and Kim H W, *Mater. Letters* **60** (2006) 3255.
116. Eizadjou M, Kazemi Talachi A, Danesh Manesh H, Shakur Shahabi H, and Janghorban K, *Compos. Sci. Tech.* **68** (2008) 2003.
117. Rafizadeh E, Mani A, and Kazeminezhad M, *Mater. Sci. Eng. A* **515** (2009) 162.
118. Shin D H, Park J J, Kim Y S, and Park K T, *Mater. Sci. Eng. A* **328** (2002) 98.
119. Khodabakhshi F, Kazeminezhad M, and Kokabi A H, *Mater. Sci. Eng. A* **527** (2010) 4043.
120. Khakbaz F, and Kazeminezhad M, *J. Manuf. Proc.* **14** (2012) 20.
121. Satheesh Kumar S S, and Raghu T, *Mater. Des.* **57** (2014) 114.
122. Satheesh Kumar S S, and Raghu T, *Mater. Des.* **32** (2011) 4650.
123. Morattaba S, Ranjbarb K, and Reihanian M, *Mater. Sci. Eng. A* **528** (2011) 6912.